CANADIAN JOURNAL OF EXPLORATION GEOPHYSICS
VOL. 28, NO 2 (DECEMBER 1992), P. 71-80

THE FILTERING CHARACTERISTICS OF LEAST-SQUARES POLYNOMIAL APPROXIMATION FOR REGIONAL/RESIDUAL SEPARATION

JEFFREY B. THURSTON[1] AND R. JAMES BROWN[2]

ABSTRACT

Least-squares polynomial approximation is essentially a low-pass digital filtering procedure that can be used to remove regional fields from potential-field data. In this paper we study the filtering characteristics of two different forms of polynomials in two independent variables. In one form of polynomial its order is equal to the highest power of any term in the polynomial (e.g., x^2, xy, and y^2 for order 2). In the second form, the order is equal to the highest power of any independent variable in the polynomial (e.g., x^2y^2 for order 2). The latter definition results in polynomials that consist of all the terms that comprise polynomials arising from the former definition, as well as higher-order cross terms.

Using orthogonal polynomials for the approximating function facilitates formulation of the computations in terms of space-variant convolution. Discrete Fourier transforms of the ensuing impulse responses give the transfer functions of least-squares polynomial approximation. These transfer functions reveal the following filtering characteristics: inherent strike sensitivity; diminishing passband flexibility for an increasing number of grid points; a bias to higher frequencies for nonsquare grids (with different numbers of points per side) along the direction with fewer points; spatial variance that leads to a general increase in passband width towards the edges of the grid; and phase distortion that, near the centre of the grid, is almost linear in the passband but deviates from linearity as the frequency and radial distance from the centre increases. Synthetic and real data examples show how these effects can induce artifacts that distort regional fields.

In light of these potential hazards, we recommend that this method, which has advantages of being simple to implement and computationally nonintensive, be used only for preliminary separation. Rather, detailed interpretation should be performed on maps processed with linear, phase-invariant digital filters.

INTRODUCTION

Potential-field data are generally subjected to a regional/residual separation procedure before interpretation is undertaken. This is done to separate the long-wavelength anomalies of the regional field, and attributed to deep and large-scale sources, from the shorter wavelength features constituting the residual field, assumed to arise from shallower, smaller-scale sources. There have been many studies describing methods used to perform this separation. Most of the techniques can be put into one of three general categories: manual smoothing; approximating the long-wavelength component of the field with a low-order polynomial; and linear digital filtering. Manual methods tend to produce the most reliable results but are time-consuming. The success of automated methods largely depends on the separability of the spectral signatures of the regional and residual fields.

Separation by least-squares polynomial approximation has been in use for over forty years (Agocs, 1951; Simpson, 1954; Swarz, 1954). More recent reviews (Wren, 1973; Davis, 1986) and refinements (Abdelrahman et al., 1985, 1989; Zeng, 1989; Beltrão et al., 1991) indicate a continued widespread use. Because the procedure effects a spectral separation, it is appropriate for one to gain an understanding of its filtering characteristics. Lance (1982) did this for the case of single-variable operators; however, to our knowledge, no such analysis has addressed the two-variable case. Our aims in this study, then, have been to examine the filtering characteristics of least-squares approximation for field data in two independent variables, and to determine what artifacts may be introduced into the regional field as a consequence of these properties.

LEAST-SQUARES POLYNOMIAL APPROXIMATION

Polynomial approximation is generally performed with a function either of the form:

$$Z(x,y) = \sum_{r=0}^{r+s \le n} \sum_{s=0} a_{rs} x^r y^s, \qquad (1)$$

Manuscript received by the Editor June 5, 1992; revised manuscript received January 5, 1993.

[1]Formerly, Department of Geology and Geophysics,The University of Calgary, Calgary, Alberta T2N 1N4; presently, Commonwealth Geophysical Development Ltd., 6620 Crowchild Trail S.W., Calgary, Alberta T3E 5R8

[2]Department of Geology and Geophysics, The University of Calgary, Calgary, Alberta T2N 1N4

We would like to thank Vadim Lyatsky for stimulating this study and for sharing his considerable knowledge of northern Alberta in general and the Trout Mountain Anomaly in particular. Thoughtful and careful reviews by Kevin Brown, Jeff MacQueen and Stephen Reford are greatly appreciated. We are grateful to Sabrina Trupia for assistance in preparation of some of the figures.

or of the form:

$$Z(x,y) = \sum_{r=0}^{n}\sum_{s=0}^{n} a_{rs}x^r y^s. \qquad (2)$$

The difference between the two is demonstrated by Table 1. Based on the shapes of these arrays of polynomial elements as they appear in Table 1, these will be referred to as the *triangular* and *square* forms of these polynomials. For either form, the order of the polynomial is said to be n. The space-domain representation provides no evidence regarding the differences that are important for regional/residual separation; however, these will become clear in the course of the forthcoming wavenumber-domain analysis. Because the following derivations apply equally to both types, the upper limits of summation have been omitted for the sake of generality.

The method of nonorthogonal polynomials

The use of nonorthogonal polynomials for least-squares approximation of potential-field data is well known (Agocs, 1951; Fajklewicz, 1959; Abdelrahman et al., 1985). Further, a detailed summary has been given by Davis (1986); hence only a cursory discussion is presented here.

It is assumed that the data, denoted $z(x_i, y_j)$, have been sampled on a rectangular grid with spatial dimension $(m\text{-}1)\Delta x$ by $(p\text{-}1)\Delta y$ where Δx and Δy are the grid intervals in the x and y directions. If $Z(x, y)$ represents the polynomial that best fits the data, then it has the form of equation (1) or (2). The coefficients a_{rs} can be determined by minimization of the mean square error, E, of the best-fit polynomial, $Z(x, y)$, relative to the observed data $z(x, y)$:

$$E = \sum_{t=1}^{m}\sum_{u=1}^{p}\left\{Z(x_t,y_u) - z(x_t,y_u)\right\}^2. \qquad (3)$$

Setting the $(n+1)(n+2)/2$ partial derivatives equal to 0, for the triangular polynomials [equation (1)], or the $(n+1)^2$ partial derivatives equal to 0, for the square polynomials [equation (2)], invokes the least-squares condition:

$$\frac{\partial E}{\partial a_{rs}} = 0, \qquad (4)$$

for all $r+s = 0, 1, 2, \ldots n$ or for $r = 0, 1, 2, \ldots n$ and $s = 0, 1, 2, \ldots n$. This generates either a system of $(n+1)(n+2)/2$ or $(n+1)^2$ normal equations that can be used to solve for the unknown coefficients of equations (1) or (2), respectively. The regional field is then given by $Z(x_i, y_j)$ and the residual by $z(x_i, y_j) - Z(x_i, y_j)$.

1	x	x^2	x^3	x^4
y	xy	x^2y	x^3y	x^4y
y^2	xy^2	x^2y^2	x^3y^2	x^4y^2
y^3	xy^3	x^2y^3	x^3y^3	x^4y^3
y^4	xy^4	x^2y^4	x^3y^4	x^4y^4

Table 1. Terms contained in the two types of approximating polynomials for $n = 4$. The triangular form [equation (1)] contains the terms that are above the dashed line, whereas the square form [equation (2)] contains all the terms in Table 1 (after Hayes, 1970).

The method of orthogonal polynomials

The method of nonorthogonal polynomials suffers from numerical instability due to the necessity of inverting a Hilbert matrix (Lapidus, 1962, p. 329). This leads to: (1) a loss of accuracy due to rounding errors and (2) computationally intensive algorithms. The preferred approach is to use orthogonal polynomials to avoid these complications. Of added importance for this study is the fact that orthogonal polynomials allow least-squares polynomial-separation calculations to be formulated as two-dimensional convolution, thus permitting wavenumber-domain analysis of the procedure. An excellent review of the use of orthogonal polynomials in approximating data in two independent variables is given by Hayes (1970). This review is summarized below, followed by a demonstration that the method is indeed equivalent to convolution.

It is possible to rewrite equations (1) and (2) in terms of the polynomials of two variables, $P_{r,s}(x, y)$ that correspond to the terms $x^r y^s$ in equations (1) and (2) and which are orthogonal over the domain of the data. If $P_{a,b}(x, y)$ and $P_{c,d}(x, y)$ are orthogonal to one another, then,

$$\sum_{t=1}^{m}\sum_{u=1}^{p} P_{a,b}(x_t,y_u)P_{c,d}(x_t,y_u) = 0 \qquad (5)$$

for $a+b \neq c+d$, where the summation limits have the same meaning as before.

Because the data are arranged on a regular rectangular grid, orthogonal polynomials in two independent variables are equivalent to the product of two single-variable orthogonal polynomials. That is, Hayes (1970) has shown,

$$P_{r,s}(x,y) = P_r(x)Q_s(y) \qquad (6)$$

for $r+s \leq n$, or $r, s \leq n$, where $P_r(x)$ and $Q_s(y)$ are both sets of orthogonal polynomials of a single variable. From a practical standpoint this is important because several algorithms have been developed for rapid generation of orthogonal polynomials in one variable. An efficient method for doing this is the recursive relationship of Forsythe (1957), by which:

$$P_{-1}(x) = 0,$$
$$P_0(x) = 1 \qquad (7)$$

and

$$P_{r+1}(x) = 2(x-\alpha_{r+1})P_r(x) - \beta_r P_{r-1}(x),$$

where

$$\alpha_{r+1} = \frac{\sum_{t=1}^{m} x_t P_r^2(x_t)}{\sum_{t=1}^{m} P_r^2(x_t)} \tag{8}$$

and

$$\beta_r = \frac{\sum_{t=1}^{m} P_r^2(x_t)}{\sum_{t=1}^{m} P_{r-1}^2(x_t)}, \tag{9}$$

and similarly for $Q_s(y)$.

Then the best-fit polynomial [equations (1) and (2)] can be rewritten as:

$$Z(x,y) = \sum_r \sum_s c_{rs} P_r(x) Q_s(y), \tag{10}$$

where the least-squares solution is given as:

$$C_{rs} = \frac{\sum_{t=1}^{m}\sum_{u=1}^{p} z(x_t, y_u) P_r(x_t) Q_s(y_u)}{\sum_{t=1}^{m}\sum_{u=1}^{p} P_r^2(x_t) Q_s^2(y_u)}. \tag{11}$$

Substituting equation (11) into equation (10) and rearranging the order of summation gives:

$$Z(x,y) = \sum_{t=1}^{m}\sum_{u=1}^{p}\sum_r\sum_s \frac{P_r(x)Q_s(y)z(x_t,y_u)P_r(x_t)Q_s(y_u)}{\sum_{t=1}^{m}\sum_{u=1}^{p} P_r^2(x_t)Q_s^2(y_u)}. \tag{12}$$

Evaluating equation (12) at $x = x_i$ and $y = y_j$ gives an expression for the best-fit polynomial at each grid point given by (x_i, y_j). This function represents the long-wavelength, or regional, component:

$$Z_{\text{reg}}(x_i, y_j) = \sum_{t=-\infty}^{\infty}\sum_{u=-\infty}^{\infty} h_{tu} z(x_{i-t}, y_{j-u}), \tag{13}$$

where h_{tu} is zero, except in the interval $1 \le t \le$ m and $1 \le u \le p$, within which:

$$h_{tu} = \sum_r\sum_s \frac{P_r(x_i)P_r(x_t)Q_s(y_j)Q_s(y_u)}{\sum_{t=1}^{m}\sum_{u=1}^{n} P_r^2(x_t)Q_s^2(y_u)}. \tag{14}$$

The calculation described by equation (13) is a two-dimensional convolution, and hence equation (14) gives the expression for the spatially variant impulse response for low-pass filtering via polynomial approximation. Equation (14) is similar to an expression given by Lance (1982).

Wavenumber-domain Response of Least-squares Approximation

The objective of the study of the wavenumber-domain response of least-squares approximation is to understand the filtering characteristics of this operation. This is done by computing discrete Fourier transforms of equation (14), which enables examination of amplitude responses, phase responses, passbands and spatial variation.

From equation (14) it can be seen that a unique convolution operator is required for each grid node and that this operator depends both upon the number of data points along each side of the grid and upon the number of terms in the approximating polynomial. Thus, a complete suite of transfer functions is prohibitively large. As a consequence, the forthcoming study focuses on an analysis of the universal characteristics of least-squares polynomial approximation derived from specific, representative examples. A focal point of this analysis is the differences in the filtering properties between the two forms of approximating polynomials. However, because square polynomials contain $(n/2)(n+1)$ more terms than triangular polynomials of the same order, a comparison of these two is hardly justifiable. However, a triangular polynomial of order 7 and a square polynomial of order 5 both comprise 36 terms. Hence, we use these orders whenever comparisons between the two polynomial types are made.

Transfer functions

Amplitude spectra for low-pass polynomial approximation filters are shown in Figures 1 and 2. These correspond to filters that operate on the central grid point of a 25x25 grid and seventh-order triangular and fifth-order square polynomials. The central grid point is the only location for which the approximating function does not alter the phase. This can be seen from equation (14), where h_{tu} is a real and even function at the centre of the grid (Thurston, 1991). The nonzero-phase response of operators corresponding to other grid locations are later discussed in more detail. Further, because the transfer function of the operator corresponding to the centre

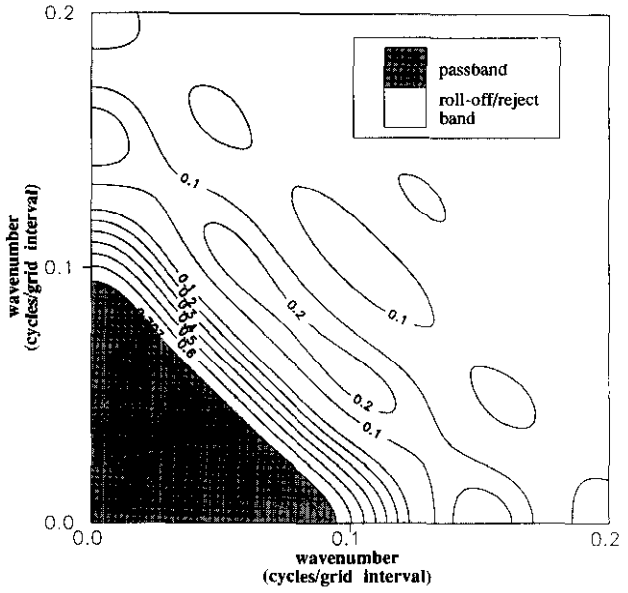

Fig. 1. Amplitude response of the least-squares polynomial approximation filter that operates on the centre node of a 25x25 grid, based on a triangular polynomial with $n = 7$.

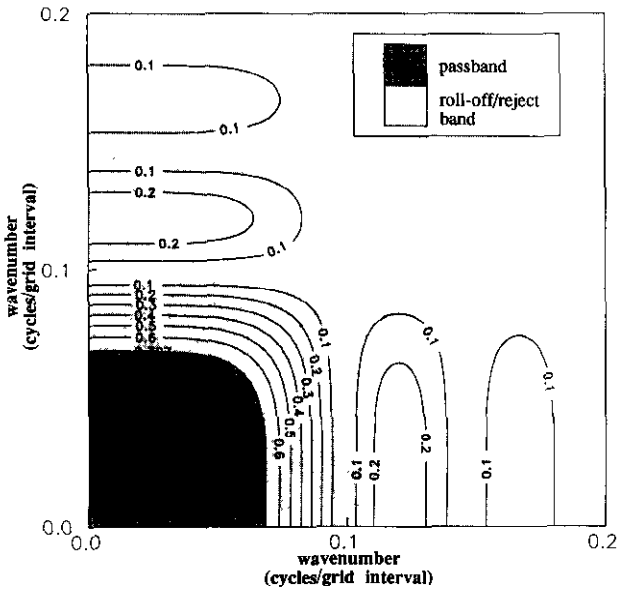

Fig. 2. Same as Figure 1, for a square polynomial with $n = 5$.

grid location is real and even, the Fourier transform is real and even. Thus, it is only necessary to show the first quadrant of the amplitude spectra.

Examination of spectra computed using several data-set sizes and polynomial orders indicates that these are representative examples and, thus, illustrate some important features of polynomial approximation. In general, as for approximation in one variable (Wood and Hockens, 1970; Chan and Leong, 1972), least-squares approximation in two variables passes all frequencies. However, the signal is effectively attenuated outside the passband, which here is taken to consist of regions where the amplitude is within 3 dB of the maximum (Meskö,1984). In addition, there is a gentle decrease in amplitude with increasing wavenumber in the passband. This rate of attenuation increases in the roll-off region and decreases in the reject region. In the reject region there are a number of side lobes of negligible amplitude. Finally, the amplitude responses are symmetric about a line defined by $k_x = k_y$. This is because the grid is square. The consequences of using nonsquare data grids are discussed later.

A detrimental characteristic of these filters is their strike sensitivity. That is, frequencies passed parallel to the axes are not the same as those along other azimuths. In Figure 1, the passband is considerably narrower along $k_x = k_y$ than it is along k_x or $k_y = 0$, while in Figure 2 it is wider along $k_x = k_y$. This is important because the Fourier transform preserves signal directivity (Fuller, 1967). Hence the high-frequency content will be reduced in the directions of the coordinate axes as compared to orientations that are oblique to the axes for square polynomials, while the opposite will apply to triangular polynomials.

Passband measurements

In order to gain an understanding of the filtering characteristics of polynomial approximation, passbands were measured for centre filters for various sizes of square data sets and polynomial orders. We did this by extracting profiles from discrete two-dimensional Fourier transforms of the impulse responses along specified orientations and determining the frequency at which the amplitude spectrum is -3 dB relative to the value at zero wavenumber. Discrete Fourier transforms were computed at increments of 0.001 cycles per grid interval, so this method determines the passband to within 0.0005 cycles per grid interval. These measurements, shown in Figure 3, are intended to give estimates of the passbands for a specified grid dimension (i.e., number of points along the sides of the grid) and polynomial order and to illustrate general trends in the variation of the cut-off wavenumber. It is important to remember that the general features apply to all grid locations; however, the actual values have less and less significance as the distance from the centre of the grid increases. This is illustrated in the forthcoming discussion regarding spatial variation.

We made the measurements by obtaining discrete Fourier transforms along profiles defined by $k_y = 0$, for $k_x \geq 0$ (i.e., along the positive k_x axis), and along $k_x = k_y$ for k_x, $k_y \geq 0$ (i.e., at an orientation of $\pi/4$ radians to the positive k_x axis). These directions were chosen in order to better understand the directional dependence. Because this analysis is for the centre of a square data grid, the transfer functions are real and even, and the results along the k_x axis are applicable to orientations parallel to either axis. Likewise, the results along $k_x = k_y$ are applicable to azimuths defined by $\pi/4 + b\pi/2$ ($b = 1, 2, \ldots$) relative to the k_x axis. In addition, it can be shown that both polynomial types have the same amplitude responses along the coordinate axes for a given n (Thurston, 1991). Hence, on Figure 3 the measurements along the axis are the same for both polynomial types.

There are three important insights that can be inferred from Figure 3.

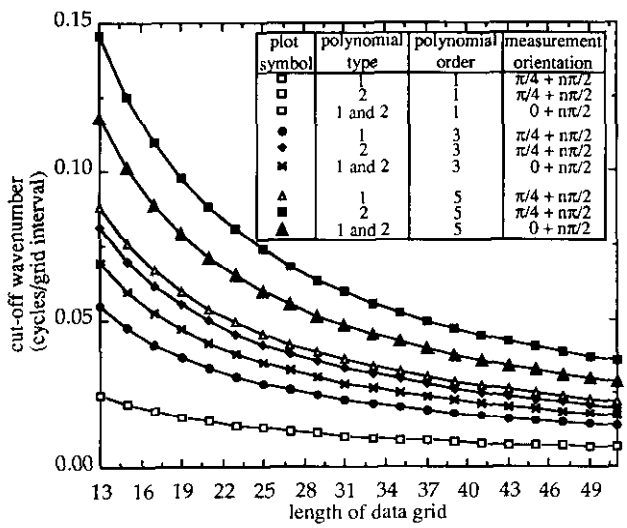

Fig. 3. Passbands for centre filters.

1) The passband width decreases with increasing data-set size and decreasing polynomial order. This effect is less pronounced as the data-set size increases. This places some limitations on the flexibility of polynomial approximation for filtering data grids with a large number of points. That is, variation of wavenumber content between grids computed from different polynomial orders decreases, and there are diminishing marginal returns on cut-off wavenumber reduction for further increases in grid size. Lance (1982) obtained similar results for data in one independent variable.
2) Based on the differences between the cut-off wavenumber parallel to, and at an angle of $\pi/4$ to, the axes, the inconsistencies in the passband width apply for varying data set sizes and polynomial orders. The orientation dependence decreases for lower orders and for an increasing number of data points. Also, this effect is less pronounced for square polynomials than it is for triangular polynomials. The potential for distortion of anomaly shape will be shown later.
3) Finally, while these results are for square data grids, some comments can be made regarding data on grids that are not square. This is possible because the amplitude response along a frequency-domain axis is affected only by the number of points along the corresponding spatial axis. Hence, while the passband measurements along $k_x = k_y$ shown in Figure 3 have no meaning for grids that are not square, the measurements along the axes do. This gives an indication of the bias inherent in approximating data on a rectangular grid. That is, high-frequency content is diminished along the side of the grid with the greater number of points. This directional bias acts in conjunction with the anisotropic nature of the passband discussed above.

Spatial variation and phase distortion

The discussion so far has been limited to transfer functions for convolution operators for centre filters. This is a restricted case, as it applies only to the central grid point of a rectangular data array containing an odd number of points along each side. One issue that must be addressed is that the passband width varies away from the central grid node. This variation is shown in Figures 4 and 5, which are contour plots of passband measurements at each grid node for a specified polynomial order, grid size and orientation. Figure 4 shows the variation along an azimuth of $\pi/4$ to the k_x axis for a 25x25 grid and a triangular seventh-order polynomial. Shown in Figure 5 are the same results for a 25x25 grid and a square fifth-order polynomial. The pattern of variation shown in Figures 4 and 5 are consistent for various orders of triangular and square polynomials. These results show that the passband generally increases as the distance from the centre of the grid increases; however, this variation is not radially symmetric. This implies that least-squares polynomial approximation biases features depending on two factors: the radial distance of the feature from the centre of the grid and the azimuth of the feature with respect to the centre of the grid.

Potential-field separation filters should be phase invariant (Syberg, 1972; Jacobsen, 1987). Hence, a second concern is that polynomial approximation may cause alteration of the phase. We have empirically determined that, unlike spatial variation in the passband, the phase shift corresponding to each grid node is only a function of the radial distance from the centre of the grid. Figure 6 shows phase responses at

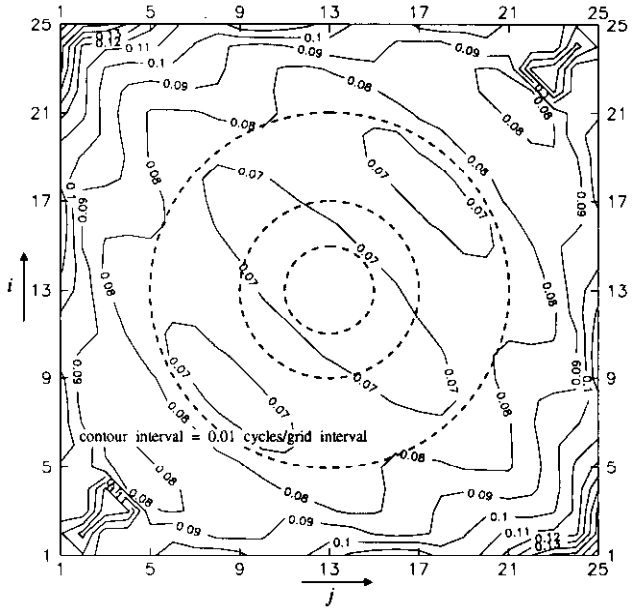

Fig. 4. Space-domain contour plot of passband variation along an azimuth of $\pi/4$ of least-squares polynomial approximation for a grid size of 25x25 and a triangular polynomial with $n = 7$. The spatial indices i (corresponding to x) and j (corresponding to y) correspond to those in equation (13). The dashed concentric circles are radii of 2, 4 and 8 grid units and show the locations of the grid nodes that correspond to the phase responses in Figure 6.

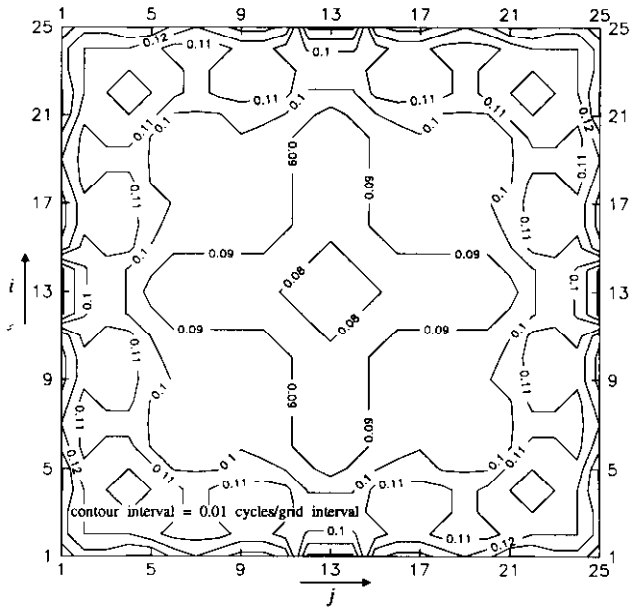

Fig. 5. Same as Figure 4, for a square polynomial with $n = 5$.

three radial distances for a triangular seventh-order polynomial and a 25x25 grid. The characteristics of these phase responses are typical of phase responses for polynomial approximation using both forms for the approximating polynomial and various orders and grid sizes. This demonstrates that polynomial approximation induces phase distortion that increases with the radial distance from the centre. Over most of the data grid the largest phase shifts occur at wavenumbers greater than the cut-off wavenumber and, within the passband, phase shifts are almost linear. This will tend to cause a bulk shift of an anomaly. On the periphery of the data grid, where the cut-off wavenumbers are greatest, phase alterations are larger and do not vary linearly within the passband.

Zurflueh (1967) noted the unreliability of polynomial approximation in the vicinity of the edges of the data. Our results indicate that these edge effects are due to the large passband variation, shown in Figures 4 and 5, and by the considerable phase distortion.

Results

The results of polynomial approximation may be evaluated in light of knowledge of the filtering characteristics. The algorithm implemented for least-squares approximation is based on computing polynomial coefficients in terms of orthogonal functions specified by equation (11). The regional field is then calculated by using these coefficients in equation (10). This has been performed on three data sets: two synthetic examples and Bouguer gravity data from north-central Alberta.

Synthetic data

Two synthetic examples are presented in order to illustrate some of the properties of polynomial approximation determined in the wavenumber-domain analysis. The first data set consists of sets of unit-amplitude trends located at various positions and oriented at 45° to the grid. Polynomial approximation of these data demonstrates the differences in the passband of the two types of polynomials, the effects of spatial variation in the passband and the effects of phase distortion. Shown in Figures 7 and 8 are the results of approximation with a triangular seventh-order polynomial and a square fifth-order polynomial. Near-linear phase distortion gives rise to the misalignment of the unit-amplitude trends and the peaks from polynomial approximation. In addition, the magnitude and the high-frequency component of the trends are greater in Figure 8 than in Figure 7. This is because of the larger passband width for square polynomials. Further, there is a discrepancy in the frequency content of trends on the same map. This is a result of spatial variation in the passband. Comparing Figure 4 with Figure 7 and Figure 5 with Figure 8 indicates that there is a correspondence between regions containing higher frequencies and regions of wider passband.

The second synthetic data example uses the rectangular parallelepiped. The purpose of this is to demonstrate the potential for shape distortion as a result of anisotropy in the passband. Shown in Figure 9 is the gravity anomaly for a 15-km × 15-km rectangular parallelepiped buried 15 km below the surface, with a thickness of 5 km. Because this example is intended to highlight the effects of passband anisotropy, the source body is located at the centre of the grid in order to minimize the effects of phase distortion and spatial variation. Figures 10 and 11 show the results of approximating this anomaly with a triangular seventh-order polynomial and a square fifth-order polynomial. The square shape in Figure 11 is a result of biasing signal oblique to the axes, whereas the

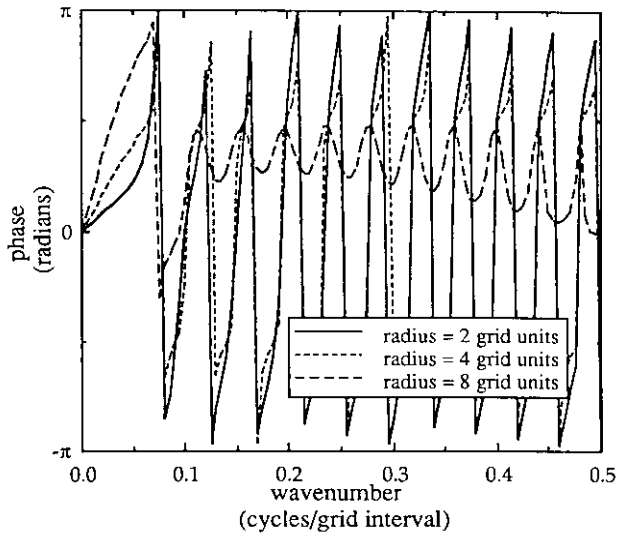

Fig. 6. Phase responses of a triangular polynomial with $n = 7$ computed along $k_x = k_y$.

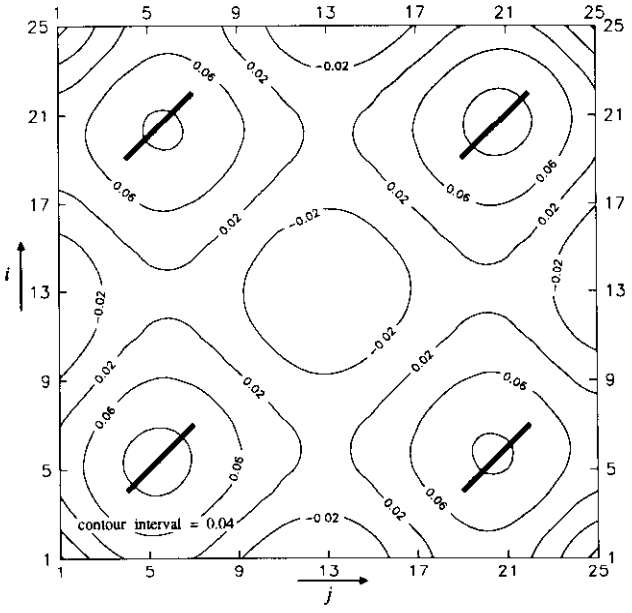

Fig. 7. Space-domain plot of approximation of unit amplitudes with a triangular polynomial with $n = 7$. The spatial indices i (corresponding to x) and j (corresponding to y) correspond to those in equation (13). The bold lines show the unit-amplitude features.

rotated square shape in Figure 10 is a result of muting such signal. Neither polynomial type reliably preserves the shape of the input data; however, the results in Figure 11 more closely resemble the input than do the results in Figure 10, where the anomaly appears to be rotated.

Real data

Filtering of a Bouguer gravity data set from north-central Alberta has been performed by polynomial approximation. The data are a subset of the Bouguer gravity anomaly map of Canada (Goodacre et al., 1987). The grid was extracted in digital form and comprises 75x75 points with a 5-km grid interval. These data are shown in Figure 12. The most prominent feature on this map is an approximately 170-km × 60-km feature trending north-south (in the northern portion) and southwest-northeast (in the southern portion), with a minimum relative value of -98 mGal. It has been named the Trout Mountain Low (Walcott and Boyd, 1971). Burwash and

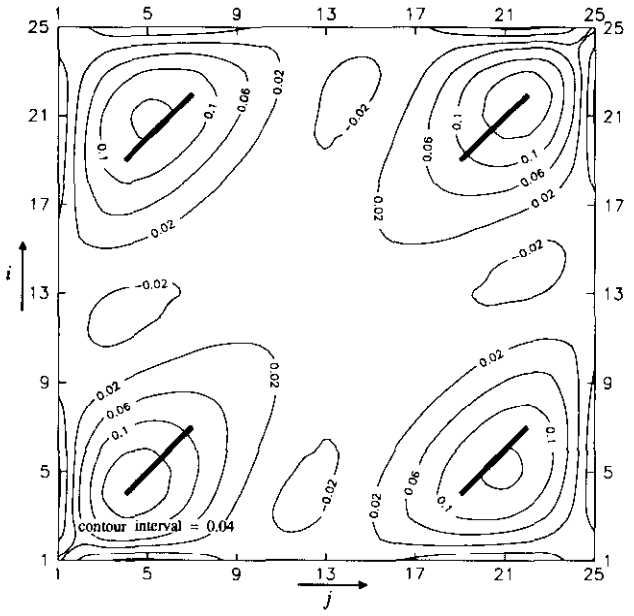

Fig. 8. Same as Figure 7 using a square polynomial with $n = 5$.

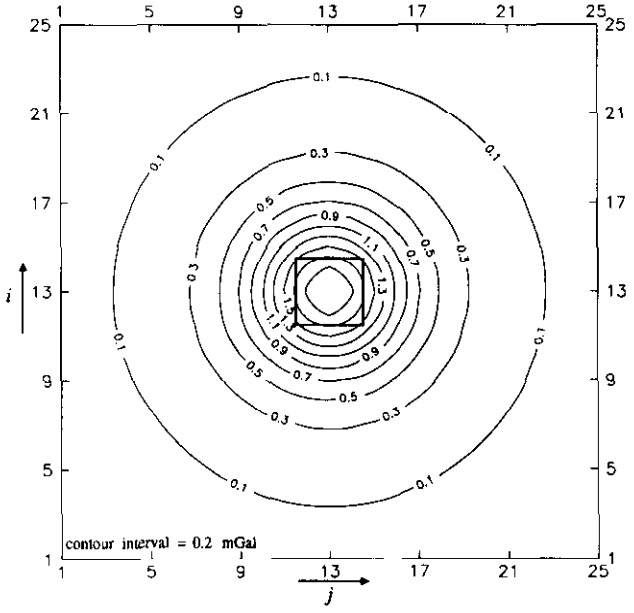

Fig. 9. Gravity anomaly of a rectangular parallelepiped. The spatial indices i (corresponding to x) and j (corresponding to y) correspond to those in equation (13). The source body is outlined by the bold square.

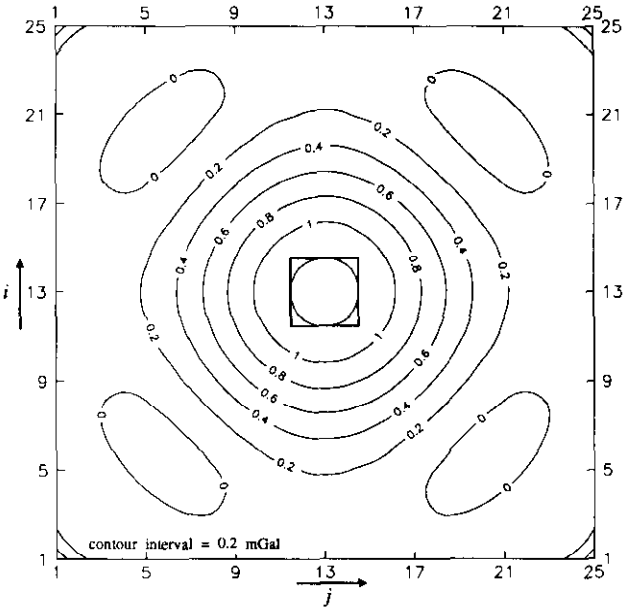

Fig. 10. Triangular polynomial with $n = 7$ computed by least-squares approximation to the anomaly in Figure 9. The spatial indices i (corresponding to x) and j (corresponding to y) correspond to those in equation (13).

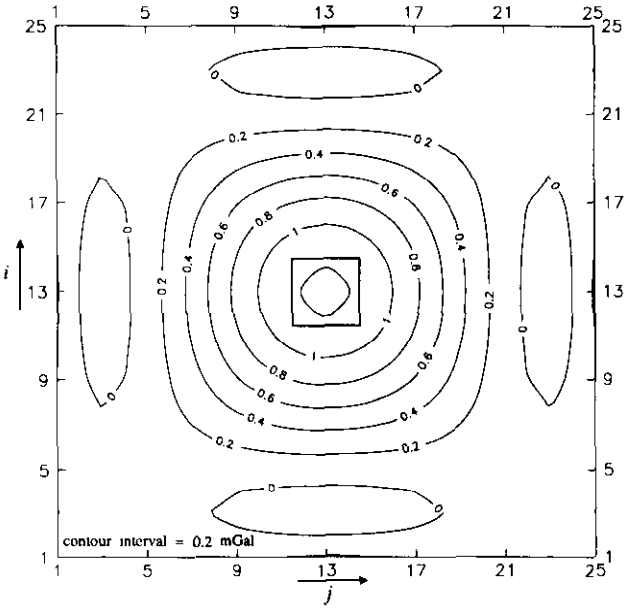

Fig. 11. Same as Figure 10, using a square polynomial with $n = 5$.

Power (1990) attribute this feature to a granitic pluton, 25 km thick, emplaced in a granulite-facies country rock. This residual low is embedded in a long-wavelength component that generally decreases to the southwest.

The long-wavelength component of the Bouguer anomaly field in this region of Alberta has been examined in a number of studies and several models have been proposed to explain its origins. Sprenke and Kanasewich (1982) imaged a relative decrease to the southwest on a middle-wavelength (500-1000-km bandpass-filtered) Airy anomaly map and attributed it to either a topographic high on the Moho or anomalously high mantle densities. Stephenson et al. (1989) resolved a gradient with a relative decrease to the southwest on a 400-700-km bandpass-filtered Airy anomaly map. This trend was thought to be due to crustal thickening beneath the Rocky Mountains. Burwash and Power (1990) ascribe the regional field in the vicinity of the Trout Mountain Low to both crustal thickening and to effects of the Peace River Arch.

For this study, a suite of low-pass filtered Bouguer anomaly maps with cut-off wavelengths ranging between 125 km and 1000 km were generated in order to separate the Trout Mountain Low from the regional field. It was found that a 250-km long-wavelength map, shown in Figure 13, removes the signature of the Trout Mountain pluton, while depicting a relative local low, near the centre of the map, superimposed on a longer-wavelength field that decreases to the southwest. This regional field can, to a certain extent, be reproduced by polynomial approximation. This illustrates the efficacy of polynomial approximation for performing a regional/residual separation. Several regional fields were computed by polynomial approximation and the results of wavelength filtering (Figure 13) were best reproduced by using $n = 3$ in equations (1) and (2). This is not surprising, as the passband measurements indicate that for a 75x75 grid with a 5-km grid interval, least-squares approximation passes wavelengths between approximately 200 and 300 km, depending upon polynomial type, orientation and grid location. The results of polynomial approximation are shown in Figures 14 and 15.

With the exception of the data near the edges of the grid, where the passbands are considerably greater, the data shown in Figures 14 and 15 generally resemble those shown in Figure 13. However, there are some important differences. For instance, the results using the triangular polynomial, shown in Figure 14, do not properly resolve the relative high near the centre of the map. This is because, as shown in Figure 13, this feature trends predominantly northeast, oblique to the grid. Because triangular polynomials degrade high-frequency features that are not parallel to the axes, this high, which comprises relatively short wavelengths, is poorly represented on Figure 14. On the other hand, square polynomials have a larger passband parallel to this regional trend. As a result, the long-wavelength component is reasonably well-reproduced on Figure 15. However, there is some discrepancy between the trends of the regional fields shown on Figures 13 and 15. This may be because the relative high on the low-pass filtered data shown in Figure 13 does not trend exactly parallel to the direction of maximum passband of the data on Figure 15. This could result in the apparent rotation of the regional field on Figure 15.

It may be argued that the regional field in Figure 15 [equation (2)] is superior to that of Figure 14 [equation (1)] because more degrees of freedom are included in its approximating polynomial. However, it can be shown that it is not possible to correctly compute a regional field, using triangular

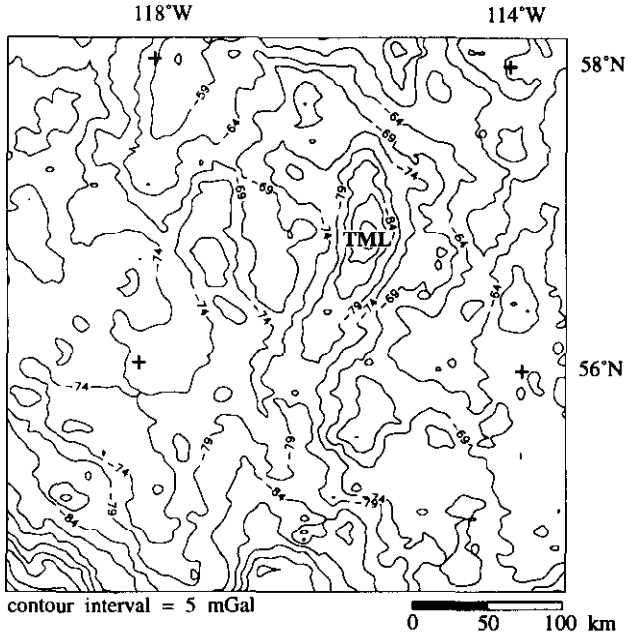

Fig. 12. Bouguer anomaly data from north-central Alberta. TML denotes the Trout Mountain Low discussed in the text.

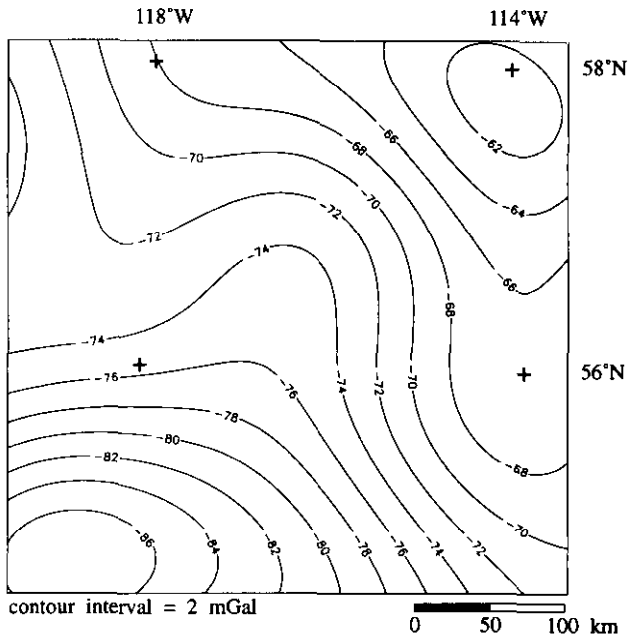

Fig. 13. The data shown in Figure 12 after low-pass filtering to eliminate wavelengths shorter than 250 km.

polynomials, that correctly depicts the long-wavelength northeast-southwest trend even if more terms are included in the approximating function. This is demonstrated by Figure 16 which shows the results of using a fourth-order triangular polynomial. Increasing the polynomial order increases the passband along the axes resulting in the inclusion of the low-frequency component of the north-south trending Trout Mountain Anomaly in the regional field.

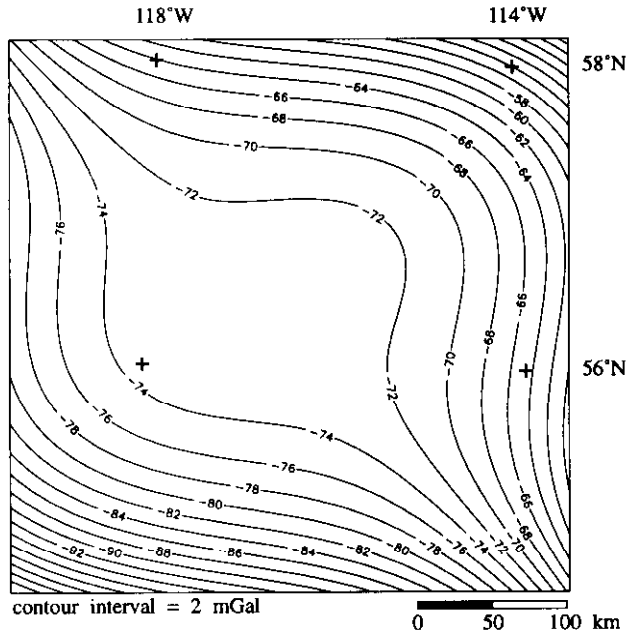

Fig. 14. Triangular polynomial with $n = 3$ computed by least-squares approximation to the data shown in Figure 12.

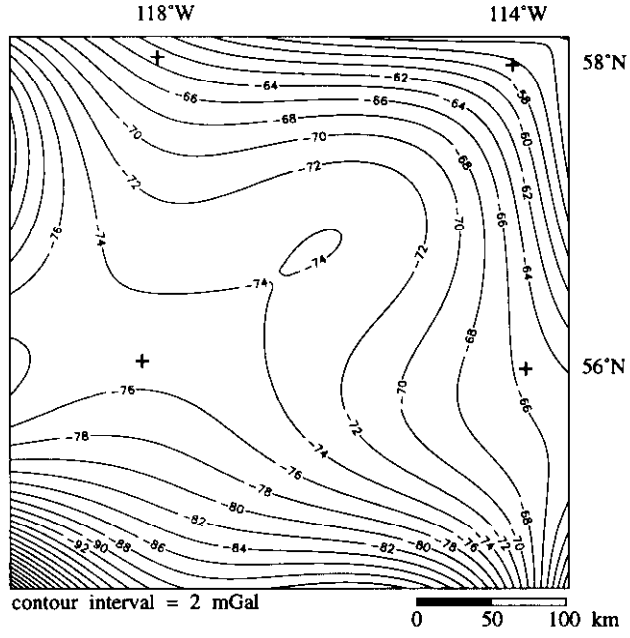

Fig. 15. Square polynomial with $n = 3$ computed by least-squares approximation to the data shown in Figure 12.

Summary and Conclusions

Determining the regional component of potential-field data usually entails suppression of high frequencies and enhancement of low frequencies. One method for doing this is least-squares polynomial approximation. We have investigated the filtering characteristics of two forms for the approximating function for least-squares approximation for data in two independent variables. To do this we formulated this operation in terms of convolution and subsequently computed Fourier transforms of the impulse responses.

This study reveals several properties that should be considered when evaluating results of this technique. These are:

1) Anisotropy in the passband. That is, the passband width varies depending upon anomaly orientation. For triangular polynomials passbands are narrower for signal oblique to the axes, whereas for square polynomials passbands are wider. The amount of anisotropy can be reduced by using more grid points and lower-order polynomials. Also, square polynomials are less anisotropic and thus may be preferable. Real and synthetic data tests suggests the anisotropy may lead to incorrect orientation of the regional field.
2) High-pass wavenumbers decrease with increasing grid size and decreasing polynomial order. The variation in passband width decreases as the size of the data array increases, limiting the flexibility of polynomial approximation for large data grids.
3) Directional bias occurs when there are unequal numbers of data points along the two sides of the grid.
4) The impulse response, and as a consequence the passband, is spatially variant.

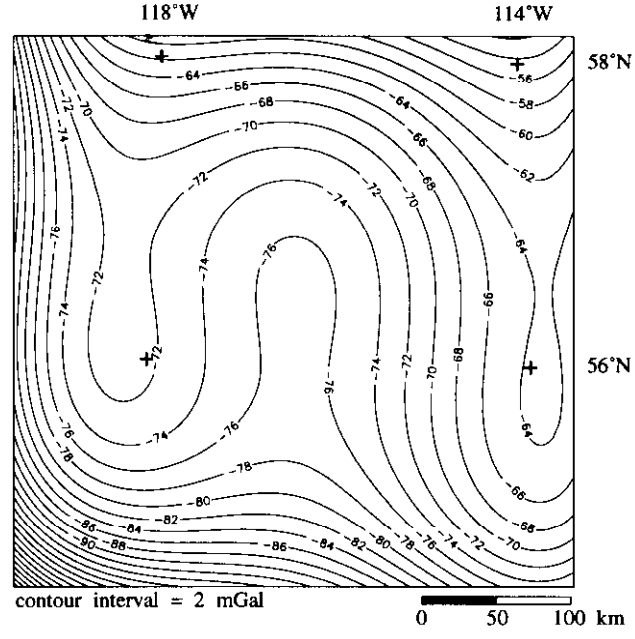

Fig. 16. Triangular polynomial with $n = 4$ computed by least-squares approximation to the data shown in Figure 12.

5) There is quasi-linear phase distortion in the passband. This distortion increases and departs from linearity as the frequency and radial distance from the centre increases. Hence, results are unreliable in the vicinity of the edges of the grid.

In light of these characteristics, we suggest that automated separation be done by linear digital filtering.

REFERENCES

Abdelrahman, E.M., Bayoumi, A.I., Abdelhady, Y.E., Gobashy, M.M. and El-Araby, H.M., 1989, Gravity interpretation using correlation factors between successive least-squares residual anomalies: Geophysics **54**, 1614-1621.

_____, Riad, S., Refai, E. and Amin, Y., 1985, On the least-squares residual anomaly determination: Geophysics **50**, 473-480.

Agocs, W.B., 1951, Least-squares residual anomaly determination: Geophysics **16**, 686-696.

Beltrão, J.F., Silva, J.B. and Costa, J.C., 1991, Robust polynomial fitting for regional gravity fitting: Geophysics **56**, 80-89.

Burwash, R.A. and Power, M.A., 1990, Trout Mountain anomaly, northern Alberta: its role in the northwest foreland of the Trans-Hudson orogeny, *in* Lewry, J.F. and Stauffer, M.R., Eds., The Early Proterozoic Trans-Hudson orogeny of North America: Geol. Assn. Can., Special Paper 37, 301-311.

Chan, S.H. and Leong, L.S., 1972, Analysis of least-squares smoothing operators in the frequency domain: Geophys. Prosp. **20**, 892-900.

Davis, J.C., 1986, Statistics and data analysis in geology: John Wiley & Sons, Inc.

Fajklewicz, Z., 1959, The use of cracovian computation in estimating regional gravity: Geophysics **24**, 465-478.

Forsythe, G.E., 1957, Generating and use of orthogonal polynomials for data-fitting with a digital computer: J. Soc. Ind. Appl. Math. **5**, 74-88.

Fuller, B.D., 1967, Two-dimensional frequency analysis and design of grid operators, *in* Mining geophysics, volume 2: theory, Soc. Expl. Geophys. 658-708.

Goodacre, A.K., Grieve, R.A.F. and Halpenny, J.F., 1987, Bouguer gravity anomaly map of Canada, *in* Canadian geophysical atlas: Geol. Surv. Can., Map 4, scale 1:10 000 000.

Hayes, J.G., 1970, Numerical approximations to functions and data: Univ. of London, The Athlone Press.

Jacobsen, B.H., 1987, A case for upward continuation as a standard separation filter for potential-field maps: Geophysics **52**, 1138-1148.

Lance, J.O., 1982, Frequency domain analysis of least squares polynomial surfaces with application to gravity data in the Pedregosa basin area: Ph.D. thesis, Univ. of Texas at El Paso.

Lapidus, L., 1962, Digital computations for chemical engineers: McGraw-Hill Book Co.

Meskö, A., 1984, Digital filtering: applications in geophysical exploration for oil: John Wiley & Sons, Inc.

Simpson, S.M., 1954, Least-squares polynomial fitting to gravitational data and density plotting by digital computer: Geophysics **19**, 808-811.

Sprenke, K.F. and Kanasewich, E.R., 1982, Gravity modelling and isostasy in western Canada: J. Can. Soc. Expl. Geophys. **19**, 255-269.

Stephenson, R.A., Zelt, C.A., Ellis, R.M., Hajnal, Z., More-à-l'Huisser, P., Mereu, R.F., Nothey, D.J., West, G.F. and Kanasewich, E.R., 1989, Crust and upper mantle structure of the origin of the Peace River Arch: Bull. Can. Petr. Geol. **37**, 224-235.

Swarz, C.A., 1954, Some geometrical properties of residual maps: Geophysics **19**, 913-928.

Syberg, F.J.R., 1972, A Fourier method for the regional/residual problem of potential fields: Geophys. Prosp. **20**, 47-75.

Thurston, J.B., 1991, Formulation of digital filters using polynomial approximation methods with applications to Bouguer gravity data from northern Alberta: M.Sc. thesis, Univ. of Calgary.

Walcott, R.I. and Boyd, J.B., 1971, The gravity field of northern Alberta and part of Northwest Territories and Saskatchewan: gravity map series, Earth Physics Branch, Energy, Mines and Resources, Canada, Nos. 103-111.

Wood, L.C. and Hockens, S.N., 1970, Least squares smoothing operators: Geophysics **35**, 1005-1019.

Wren, E.A., 1973, Trend surface analysis – a review: J. Can. Soc. Expl. Geophys. **9**, 39-44.

Zeng, H., 1989, Estimation of the degree of polynomial fitted to gravity anomalies and its applications: Geophys. Prosp. **37**, 959-973.

Zurfluch, E. G., 1967, Application of two-dimensional linear wavelength filtering: Geophysics **32**, 1015-1035.